Bioactive Materials 6 (2021) 2881–2893

Contents lists available at ScienceDirect

Bioactive Materials

journal homepage: www.sciencedirect.com/journal/bioactive-materials

Biopolymer-nanotube nerve guidance conduit drug delivery for peripheral nerve regeneration: *In vivo* structural and functional assessment

Ohan S. Manoukian [a,b], Swetha Rudraiah [b,c], Michael R. Arul [b], Jenna M. Bartley [d], Jiana T. Baker [b], Xiaojun Yu [e], Sangamesh G. Kumbar [a,b,*]

[a] Department of Biomedical Engineering, University of Connecticut, Storrs, CT, USA
[b] Department of Orthopedic Surgery, University of Connecticut Health, Farmington, CT, USA
[c] Department of Pharmaceutical Sciences, University of Saint Joseph, Hartford, CT, USA
[d] Department of Immunology, Center on Aging, University of Connecticut Health, Farmington, CT, USA
[e] Department of Biomedical Engineering, Stevens Institute of Technology, Hoboken, NJ, USA

ARTICLE INFO

Keywords:
Peripheral nerve regeneration
Nerve guidance conduit
Sciatic nerve transection
Small-molecule drug delivery
Neurotrophic factor
Functional recovery

ABSTRACT

Peripheral nerve injuries account for roughly 3% of all trauma patients with over 900,000 repair procedures annually in the US. Of all extremity peripheral nerve injuries, 51% require nerve repair with a transected gap. The current gold-standard treatment for peripheral nerve injuries, autograft repair, has several shortcomings. Engineered constructs are currently only suitable for short gaps or small diameter nerves. Here, we investigate novel nerve guidance conduits with aligned microchannel porosity that deliver sustained-release of neurogenic 4-aminopyridine (4-AP) for peripheral nerve regeneration in a critical-size (15 mm) rat sciatic nerve transection model. The results of functional walking track analysis, morphometric evaluations of myelin development, and histological assessments of various markers confirmed the equivalency of our drug-conduit with autograft controls. Repaired nerves showed formation of thick myelin, presence of S100 and neurofilament markers, and promising functional recovery. The conduit's aligned microchannel architecture may play a vital role in physically guiding axons for distal target reinnervation, while the sustained release of 4-AP may increase nerve conduction, and in turn synaptic neurotransmitter release and upregulation of critical Schwann cell neurotrophic factors. Overall, our nerve construct design facilitates efficient and efficacious peripheral nerve regeneration via a drug delivery system that is feasible for clinical applications.

1. Introduction

Every year, more than half a million Americans suffer from peripheral nerve injuries (PNI) that require surgical treatments totaling close to $2 billion in healthcare costs [1], but many continue to experience pain and/or poor functionality [2]. PNI is a common condition that results from laceration, stretch, and/or compression of the delicate peripheral nerves. The peripheral nervous system is composed of 43 nerve pairs that branch off from the central nervous system of the brain and spinal cord. Injury to these fragile nerves can result in broad-ranging symptoms depending on the severity and location, including loss of sensory, motor, and autonomic functions [2].

Although PNI is well documented and much knowledge exists on its medical conditions, treatments that provide full functional recovery are infrequent, especially for severe PNI. These severe PNI are typically characterized by large gaps >5 mm that are unable to regenerate on their own without surgical intervention [3]. The main treatments for PNI involve surgical implantation of autografts or allografts, but these are frequently limited in availability and potentially cause immunosuppression, donor site morbidity, scarring, neuroma formation, and sensory loss [4]. Tissue engineering approaches for nerve repair and regeneration, which use scaffolds, cells, and/or growth factors, can be effective alternatives to biological grafts [5,6]; however, due to limits on the size of the nerve gap that can be repaired [7,8], poor biocompatibility, and inefficient stimulation of nerve regeneration [9,10], they are often not used or only used in specific cases. Ineffective PNI repair – a potential outcome for all current treatments – can cause severe loss of sensory and/or motor function [4], and more severe damage is

Peer review under responsibility of KeAi Communications Co., Ltd.
* Corresponding author. Department of Orthopedic Surgery, The University of Connecticut, Farmington, CT, 06030- 4037, USA.
E-mail address: kumbar@uchc.edu (S.G. Kumbar).

https://doi.org/10.1016/j.bioactmat.2021.02.016
Received 18 January 2021; Received in revised form 12 February 2021; Accepted 12 February 2021

associated with slower recovery, highlighting an unmet need for better treatments. Chemical [11] and electrical stimulation [12] have the ability to enhance endogenous nerve regeneration in less severe PNI injuries, and may have utility in severe PNI repair. Therefore, efforts are being made to combine the design flexibility and on-demand availability of synthetic scaffolds with robust and consistent stimulation of endogenous nerve repair mechanisms to address current treatment limitations and ultimately enhance functional outcomes of large-gap PNI repair in humans [11–13].

Immediately following nerve injury, the process of endogenous repair and regeneration is initially marked by Wallerian degeneration, which involves morphological and biochemical changes to support new growth. Regeneration at the proximal stump begins within the first 48 h, where growing axons attempt to bridge the injury gap and reinnervate with the distal target organ [14]. However, this process is extremely slow, with axon growth reported to be ~1 mm/day in humans, and the endogenous repair often cannot sustain itself beyond 12 months [15,16]. In the case of a critical-size nerve defect, where the lesion extends far from the proximal end of the intact axon, regeneration to the distal stump is vitally slow and usually incomplete, and there is great risk of traumatic neuroma formation. Typically, injuries that result in nerve gaps >5 mm cannot achieve complete regeneration naturally [3]. As such, surgical intervention is required for more optimal recovery, necessitating either biological autografts or biomaterial engineered constructs, known as nerve guidance conduits (NGCs) [6,12,13]. For example, Bozkurt et al. reported on the creation of a collagen scaffold with aligned microchannels and carried out an *in vitro* assessment by culturing murine Schwann cells [17]. This study reported that cells did not attach to the scaffold but migrated along the pores and formed columns that resembled "Bands of Büngner", critical for guiding new axons during regeneration [17]. However, these scaffolds lacked the tunable mechanical and drug delivery properties critical to repair and enhance the rate of nerve regeneration [5,11,12,18,19].

To overcome some of the limitations associated with NGCs, we continue to develop and explore novel-structured bioengineered scaffolds and strategies, including the delivery of electrical and chemical cues for repairing large-gap PNI [5,11,12,18,19]. Delivering growth factors or cells with scaffolds can stimulate nerve regeneration processes, but chemical and electrical stimulation may have similar and additional benefits with fewer limitations. Neurotrophins such as nerve growth factor (NGF) and brain-derived neurotrophic factor (BDNF) can improve nerve regeneration [20–22], but proteins can have high dose requirements, short half-lives, high costs, and undesired side effects [5]. Schwann cells and other neuronal support cells can accelerate nerve regeneration as well [23], but delivering viable cells can be cumbersome and costly. No efforts have been made to encourage infiltration of endogenous Schwann cells using a drug or any other external cue to improve large-gap PNI.

Chemical stimulation with the potassium-channel blocker 4-aminopyridine (4-AP) can restore the myelination of demyelinated nerves in multiple sclerosis – most likely through its ability to prolong action potentials and amplify neurotransmitter release [24–27]; myelin ensheathes axons and acts as an electrical insulator, greatly speeding up action potential conduction [28]. Application of 4-AP to nerve crush injuries – where axons are intact but the myelin sheath is damaged – can also increase remyelination and nerve conduction velocity, leading to functional recovery [29–31]. Therefore, 4-AP has potential to enhance large-gap PNI repair, but local application in large-gap PNI and its effects on regeneration and functional recovery have not been studied.

In our previous work, we showed that 4-AP induces increased expression of neurotrophins in human Schwann cells *in vitro* in a dose-dependent manner [19]. Human Schwann cells cultured for 14 days with varying doses of 4-AP presented increased expression of NGF, myelin protein zero (P0), and BDNF neurotrophins with the increase in dose [19]. These neurotrophins promote axon regeneration, remyelination, and motor function recovery [28,32–35]. Therefore, in our work we studied the effects of short- and long-term 4-AP exposure on Schwann cells seeded on scaffolds *in vitro* and *in vivo* [19]. We understood that 4-AP can be a convulsant at improper dosages [36], but reasoned that sustained release of 4-AP within therapeutic ranges at the site of injury should ensure positive nerve regeneration without negative effects. However, controlled release of 4-AP using a scaffold is challenging, due to its low molecular weight and high aqueous solubility. Therefore, we employed a composite of chitosan and halloysite nanotubes (HNT) to design an NGC with appropriate physicochemical, structural, and drug-elution properties [19]. In brief, 600–900 nm HNT were filled with 4-AP and uniformly dispersed in IC chitosan solution to fabricate porous scaffolds [19]. Such a composite allowed encapsulation of 4-AP in the open lumens of HNT nanotubes, and closed tube endings in the chitosan enabled long-term sustained release of 4-AP [19]. We also conducted a preliminary *in vivo* study to determine the feasibility of surgically implanting these scaffolds and to evaluate biocompatibility. Upon visual and histological evaluation after 4 weeks, we found that scaffolds remained in the implantation site, had sufficient strength to withstand ambulatory forces during healing, and began regenerating the damaged nerve [19]. While these results were promising, they were merely the first step in evaluating the potential of our NGC in nerve healing.

Therefore, in our current study, we performed longer-term comprehensive *in vivo* assessments of structural and functional recovery, of our NGC conduits with and without 4-AP and the autografts. We initially characterized our bioengineered NGC for its mechanical strength, pore properties, and long-termer 4-AP release (8 weeks vs 1 week previously) *in vitro* to ensure it had the necessary properties for *in vivo* nerve regeneration testing. Our 4-AP drug-loaded conduits were tested for the ability to bridge a critical-size (15 mm) sciatic nerve defect in Wistar rats *in vivo*, by comparing to several controls, including the gold-standard autograft, non-drug-loaded conduit, and sham surgery. The effects of repair and regeneration, including myelination, were evaluated over a period of 8 weeks using several tests and assessments including electron microscopy, various histology techniques, and walking track analysis for functional motor recovery. The primary focus of our *in vivo* study was to establish the benefits of novel NGC-enabled 4-AP release and its ability to achieve functional tissue regeneration compared with the current gold-standard autograft treatment.

2. Materials and methods

2.1. Materials

Chitosan (high molecular weight), HNTs, and epichlorohydrin were purchased from Sigma-Aldrich (St. Louis, MO). Glacial acetic acid and phosphate-buffered saline (PBS) were purchased from Fisher Scientific (Fair Lawn, NJ). 4-Aminopyridine (>99%) was purchased from Alomone Labs (Jerusalem, Israel). S100B antibody was purchased from Invitrogen (Grand Island, NY). Neurofilament-H (NF–H) was purchased from Cell Signaling Technology (Beverly, MA). All surgical tools were purchased from Fine Science Tools (Foster City, CA). Neutral buffered formalin, sodium hydroxide pellets, and Vicryl® suture were purchased from Fisher Scientific Company (Suwannee, GA). Nylon monofilament suture was purchased from McKesson Medical Surgical (Cheshire, CT). Distilled (DI) water was obtained from a Millipore MilliQ system (EMD Millipore, Burlington, MA).

2.2. HNT drug loading

Drug loading of 4-AP into HNTs was achieved following the detailed methodology presented in an earlier publication [19]. A 4-AP-saturated solution was produced by dissolving 4-AP in ultrapure DI water at a concentration of 50 mg/mL at room temperature. Following dissolution, dry HNT was mixed with the 4-AP-saturated solution in a weight ratio of 1:2. To encourage better dispersion and prevent precipitation,

ultrasonication was employed for 1 h. Cyclic vacuum pumping in/out was employed to enhance the replacement of air in the HNT's internal lumen with saturated liquid [37]. Post-centrifugation, HNT-4-AP powder was collected and freeze-dried for 24 h to obtain dry powder.

2.3. Fabrication of composite NGCs

High molecular weight chitosan (3.0% w/v) was dissolved in 2% (v/v) acetic acid solution at 50 °C in a water bath. The chitosan solution was stirred overnight until a homogenous solution was obtained. Air remaining in the solution was removed by vacuum pump for 24 h. The NGC fabrication using a unidirectional freezing technique is presented in the Schematics 1. The homogenous solution was then poured into custom molds and subjected to unidirectional freezing, as described in detail in a previous publication [19]. Briefly, the molds were submersed in a 5 cm-deep pool of liquid nitrogen, creating an uni-axial thermal gradient, which resulted in unidirectional freezing of the chitosan solution. Similarly, samples with HNT-4-AP were fabricated with the addition of 5.0% (w/w) of dry powder to the stirring chitosan solution. The freezing and lyophilization of HNT-4-AP scaffolds were identical to that of neat chitosan conduits. Post-lyophilization, conduits were chemically crosslinked using alkaline epichlorohydrin solution (ECH; 0.01 mol/L) in NaOH solution (0.067 mol/L). Samples were rinsed thoroughly with DI water three times to remove unreacted ECH [19].

2.4. Physicochemical properties of the NGC

Images of the conduit porous architecture and microstructure were captured using a JEOL JSM-6335F scanning electron microscope (SEM) (JEOL USA, Inc., MA, USA). Pore properties were analyzed from the SEM images using ImageJ. Scaffolds were tested for kink resistance to ensure their stability by bending the hydrated NGC between 80° and 160° [38]. Suture retention strength was assessed using an Instron mechanical tester in the tensile mode. Finally, *in vitro* 4-AP release studies in PBS at 37 °C and hydration of the scaffolds was conducted as per our prior publication [19], but over a period 8 weeks in this study. For all these measurements, a sample size of n = 5 was used and the data are presented as mean ± standard deviation (SD).

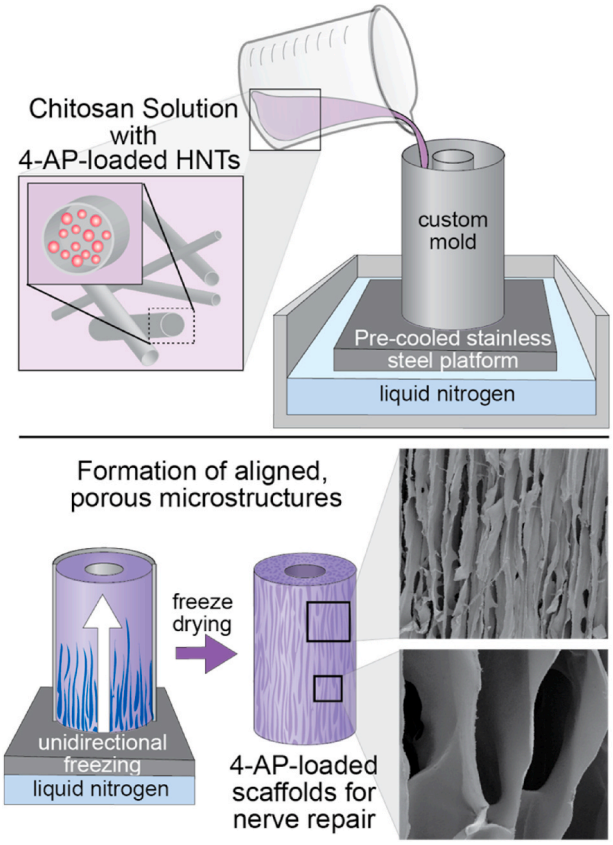

Scheme 1. The fabrication process of chitosan-halloysite nanotube composite NGCs with longitudinally aligned microchannels for the delivery of therapeutic agents.

2.5. Animal subjects

Forty [40] female Wistar rats (Charles River Laboratories, Wilmington, MA) weighing approximately 200 g each were randomly divided into four groups: sham (control), autograft repair, conduit repair, and drug-conduit repair. All animals were housed in pairs with free access to food and drinking water in a temperature-controlled room with a 12-h light-dark cycle. All animals were allowed to acclimate to housing conditions for at least one week prior to surgery. All animals were maintained and cared for according to methods approved by the Institutional Animal Care and Use Committee (IACUC) at the University of Connecticut.

2.6. Surgical procedure

Animals were anesthetized by inhalation of 2.5% isoflurane carried in medical-grade oxygen to induce and maintain a surgical anesthetic plane. The right hind leg was shaved and cleaned using betadine and isopropyl alcohol. Body temperature was maintained at approximately 37 °C by placing the animal on a surgical warming pad. All surgical procedures were conducted under aseptic conditions using sterile tools. A 30 mm incision was made parallel to the femoral axis and the right sciatic nerve was exposed through a gluteal muscle splitting incision (Fig. 1). The sciatic nerve was carefully dissected free of surrounding tissues and a 15 mm nerve segment was sharply transected and removed. For conduit and drug-conduit groups, a 20 mm conduit was secured to the proximal and distal stumps using 8–0 nylon monofilament suture (Ethicon Inc., Somerville, NJ), with approximately 2.5 mm of nerve stump inside the conduit. For autograft groups, the transected nerve segment was reversed and repaired using 8–0 nylon monofilament sutures. The muscle and skin incisions were closed with 5–0 Vicryl® suture (Ethicon Inc., Somerville, NJ). In sham-operated animals, the sciatic nerve was surgically exposed, as mentioned above, without any injury to the nerve. Pain was managed using a multi-modal analgesic approach with injections of buprenorphine every 12–18 h for two days post-operation and injections of meloxicam every 24 h for three days post-operation. A saturated solution (1.3%) of aqueous picric acid (2,4,6-trinitrophenol, Sigma-Aldrich Co., St. Louis, MO) was applied to the denervated foot immediately after surgery, and twice a week for a month, to deter scratching and biting [39,40]. At eight weeks post-operation, animals were euthanized by CO_2 asphyxiation.

2.7. Walking track analysis and sciatic functional index (SFI)

Walking track analysis was performed with the DigiGait imaging and analysis system (Mouse Specifics, Inc., Framingham, MA) to assess functional recovery following sciatic nerve transection and repair. The DigiGait system uses unique ventral plane video imaging to generate computerized paw prints while the animal walks on a speed-controlled motorized treadmill belt (Fig. 2a). The dynamic gait signal is corrected for optimizing signal-to-noise ratio and digitized to analyze and define a wide variety of gait parameters, including SFI, paw area, stance, and stride (Fig. 2b).

To assess the functional recovery of sciatic nerve damage and repair, we used SFI, which is well established in the literature for a variety of studies aimed at peripheral nerve regeneration [41–44]. SFI is determined by comparing the geometric representation of the affected hind paw from an injured rat, and comparing it to the contralateral paw. To

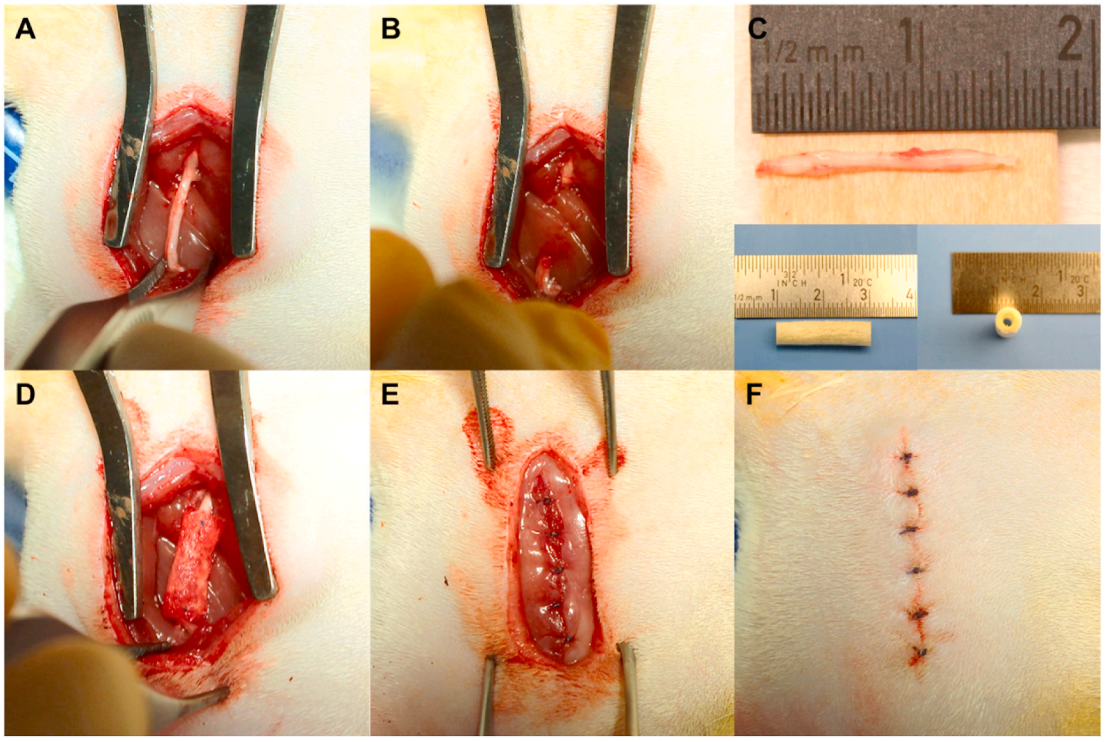

Fig. 1. Wistar rat critical-size sciatic nerve transection surgery with repair using a composite conduit. (*A*) A 30 mm incision was made parallel to the femoral axis and the right sciatic nerve was exposed through a gluteal muscle splitting incision. (*B*) A 15 mm (critical-size) segment of nerve was measured, sharply transected, and removed, creating a segmental defect. (*C*) Top: The transected 15 mm sciatic nerve segment. Bottom: The conduit is shown pre-implantation, measuring 20 mm long with a 5 mm diameter. (*D*) A 20 mm sterile conduit is sutured to proximal and distal ends of the nerve. (*E, F*) The gluteal muscle and skin incisions, respectively, are sutured closed and the incision site is cleaned.

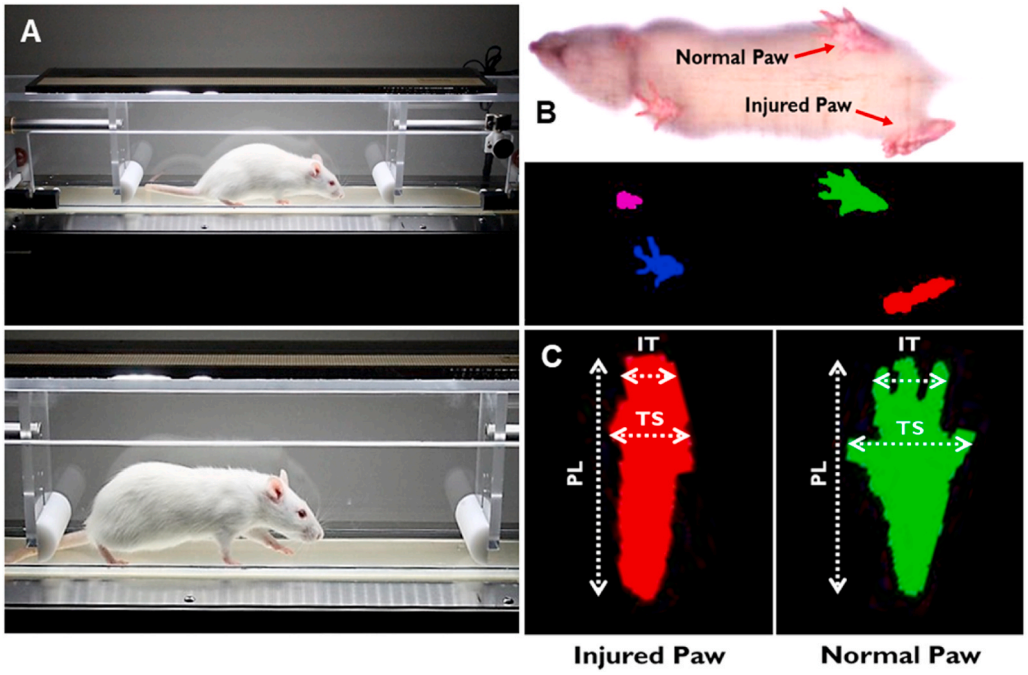

Fig. 2. The DigiGait automated treadmill system performs walking track analysis to quantify differences associated with injury severity. (*A*) A surgically-operated Wistar rat walking on the enclosed treadmill within the DigiGait system. (*B*) A ventral high-speed camera records walking, and software digitizes the footprints in preparation for walking track analysis. (*C*) Differences in several animal paw measurements can differentiate between injured (left; red) and normal (right; green) paws. Measurements such as inter-toe (IT, 2–4, distance), toe spread (TS, 1–5, spread), and paw length (PL) are used to calculate values such as the sciatic functional index (SFI). (For interpretation of the references to color in this figure legend, the reader is referred to the Web version of this article.)

calculate SFI, the following equation is used, where EPL is the experimental print length, NPL is the normal print length, ETS is the experimental toe spread, NTS is the normal toe spread, EIT is the experimental intermediary toe spread, and NIT is the normal intermediary toe spread (Fig. 2c) [45]:

$$SFI = -38.3 \times \left(\frac{EPL - NPL}{NPL}\right) + 109.5 \times \left(\frac{ETS - NTS}{NTS}\right) + 13.3 \times \left(\frac{EIT - NIT}{NIT}\right) - 8.8$$

Animals were individually placed on the DigiGait treadmill several

times to acclimate them with the apparatus prior to surgery. Baseline DigiGait data were collected for all animals prior to surgery. Following surgery, animals were tested on the DigiGait treadmill every two weeks for eight weeks using an optimal speed of 20 cm/s. Data were saved when animals walked consistently for at least 5 s, resulting in ~15 complete strides. Animals were then returned to their paired housing cages.

2.8. Transmission electron microscopy (TEM)

Axonal regeneration was investigated by transmission electron microscopy (TEM, HITACHI H −7650) in the middle regions of the regenerated sciatic nerves. Samples were fixed in 2.5% glutaraldehyde in 0.1 M phosphate buffer (pH 7.4) for 4 h at room temperature, then overnight at 4 °C. Samples were post-fixed with 1% osmium tetroxide, dehydrated, and embedded using Poly/Bed 812 embedding kit (Polysciences Inc., Warrington, PA). Ultrathin sections of 70 nm were cut, stained with uranyl acetate and lead citrate, and then examined by TEM. The axon diameter, myelinated nerve fiber diameter, and thickness of myelin sheath was evaluated using ImageJ software. For each specimen, three images were taken. The G-ratio, used to quantitatively assess myelin, was calculated according to the following equation, where D_o is the outer diameter of the corresponding fiber and D_i is the inner axon diameter:

$$G-ratio = D_i/D_o$$

2.9. Histological evaluation

Post-euthanasia, the right sciatic nerve was harvested and washed with PBS before being transferred to a histological container filled with 10% neutral buffered formalin and fixed at 4 °C overnight. Samples were then washed with PBS and transferred to 70% ethanol prior to embedding. Samples (n = 3) were embedded in paraffin and the middle region of the regenerated nerve (center of the conduit or autograft) was cut to approximately 5 μm thick slices in preparation for histological assessments. Following standard protocols, Luxol fast blue (LFB) staining was performed on sectioned slices of sham-operated and repaired nerves. Similarly, immunohistochemistry staining was performed for S100 and Neurofilament-H (NF–H, NF200) markers. Histology slides were imaged using an Aperio CS2 high-resolution digital slide scanner (Leica Biosystems Inc., Buffalo Grove, IL) and all quantification was performed using ImageJ software and a minimum of 5 images per group. Liver tissues were also harvested, fixed, and stained for hematoxylin and eosin (H&E) to assess any potential accumulation and toxicity of HNTs in the rat liver.

2.10. Data presentation and statistical analysis

All data were analyzed using Microsoft Excel and GraphPad Prism 7 (GraphPad Software, Inc. La Jolla, CA). Data were analyzed via one-way analysis of variation (ANOVA) with Tukey's posthoc corrections for multiple comparisons and reported as mean ± SD with the exception of gait data. Gait data, excluding SFI, are expressed as a ratio between the ipsilateral (right) hind paw and contralateral (left) hind paw times 100% and reported as mean ± standard error of the mean (SEM). Gait data were analyzed via two-way repeated measures ANOVA (time x group) with Tukey's posthoc corrections for multiple comparisons tests as appropriate. All statistical analyses were performed with a confidence level of 95% ($\alpha = 0.05$) using GraphPad Prism 7.

3. Results

3.1. Physicochemical property characterization of NGCs

Several assays were performed to characterize NGC properties *in vitro* to prepare for *in vivo* studies. The morphology of conduits with aligned microchannels was imaged and observed using SEM. Conduits showed ultra-porous microstructures with elliptical pores of an average diameter size of 59.3 ± 14.2 μm (mean ± SD) (Fig. 3A). The elliptical geometry is an expected result of the anisotropic growth of ice crystals during the unidirectional freezing process, and is explained in our previous publication [19]. SEM images confirmed highly aligned pores that formed longitudinal microchannels, with fenestrations interconnecting the channels (Fig. 3A). Topographically, the microstructure and architectural environment of the conduits were within range for what has been shown to be optimal for maximum axon penetration and minimum axon misdirection [17,46]. Scaffolds were able to regain their original shape after being bent through a series of angles, confirming its kink resistance (Fig. 3B, Left panel) [47]. Additionally, NGCs presented a suture retention strength ranging 18–20 N, as determined by tensile testing [19]. The NGCs with HNTs resulted in high tensile modulus of ~0.33 MPa (compared to neat chitosan with ~0.18 MPa), which is ideal for critical-sized nerve defect repair (Fig. 3B, Right panel) [19]. Previously, we showed the successful drug loading of 4-AP into HNTs using thermal gravimetric analysis (TGA) [19]. The loading of 4-AP within HNTs was confirmed in this study by using a measure of thermal degradation peaks comparing samples of neat 4-AP, neat halloysite, and 4-AP-loaded halloysite. TGA derivative curves indicated a 7.69 wt% drug-loading within HNTs, well within the 5–10 wt% range established in the literature as successful drug loading of unmodified HNTs [19,48]. NGCs were able to provide a sustained release of 4-AP over a period of 8 weeks (Fig. 3C), longer than our previous report but with a similar initial burst release [19]. The drug release pattern mirrored the NGC hydration indicating the release was diffusion-based (Fig. 3C). NGCs maintained their intact structure and were completely hydrated by 2 weeks, further attesting their suitability for *in vivo* testing (Fig. 3C).

3.2. Animal surgeries for the rat sciatic nerve defect model

We used the 15 mm critical-size Wistar rat sciatic nerve model to compare 4-AP drug-loaded NGCs, non-drug (neat) NGCs, and autograft, a sham surgery animals (Fig. 1). Autograft repair animals as well as sham-operated animals served as controls. Surgery involved transection of a 15 mm nerve and reversing nerve and suturing for autograft or suturing a 20 mm conduit (+/− 4-AP), as in our previous study [19]. Post-surgery, there were no obvious signs of systemic or regional inflammation and no surgical complications were reported with all animals surviving surgery.

One noteworthy complication was autotomy or automutilation by the rats. This is a well-described phenomenon of the rat sciatic nerve model where severing and resection of the sciatic nerve results in numbness of the foot and the rats often chew off the toes of their denervated foot, thus preventing meaningful walking track data [40,49–51]. This autotomy behavior is postulated to be associated with paresthesias, similar to phantom limb pain [50], and has been historically shown to affect 50–100% of rats undergoing sciatic nerve transection, depending on the strain [52]. Unfortunately, despite the well-established literary nature of autotomy in rat sciatic nerve models, this complication is often not declared in nerve regeneration studies. For the purposes of our study, all animals were intensively monitored and examined for signs of autotomy, and rats with severe wounds were excluded from the study. A few animals were excluded in the study and we added additional animals to make for the exclusion.

3.3. Functional recovery evaluation

3.3.1. Sciatic functional index (SFI)

The recovery of hindlimb motor function was assessed using walking track analysis evaluating a number of gait parameters, SFI in particular, biweekly over the 8-week test period. Quantitative assessment of SFI ranges from ~0 to −100, indicating normal function to complete

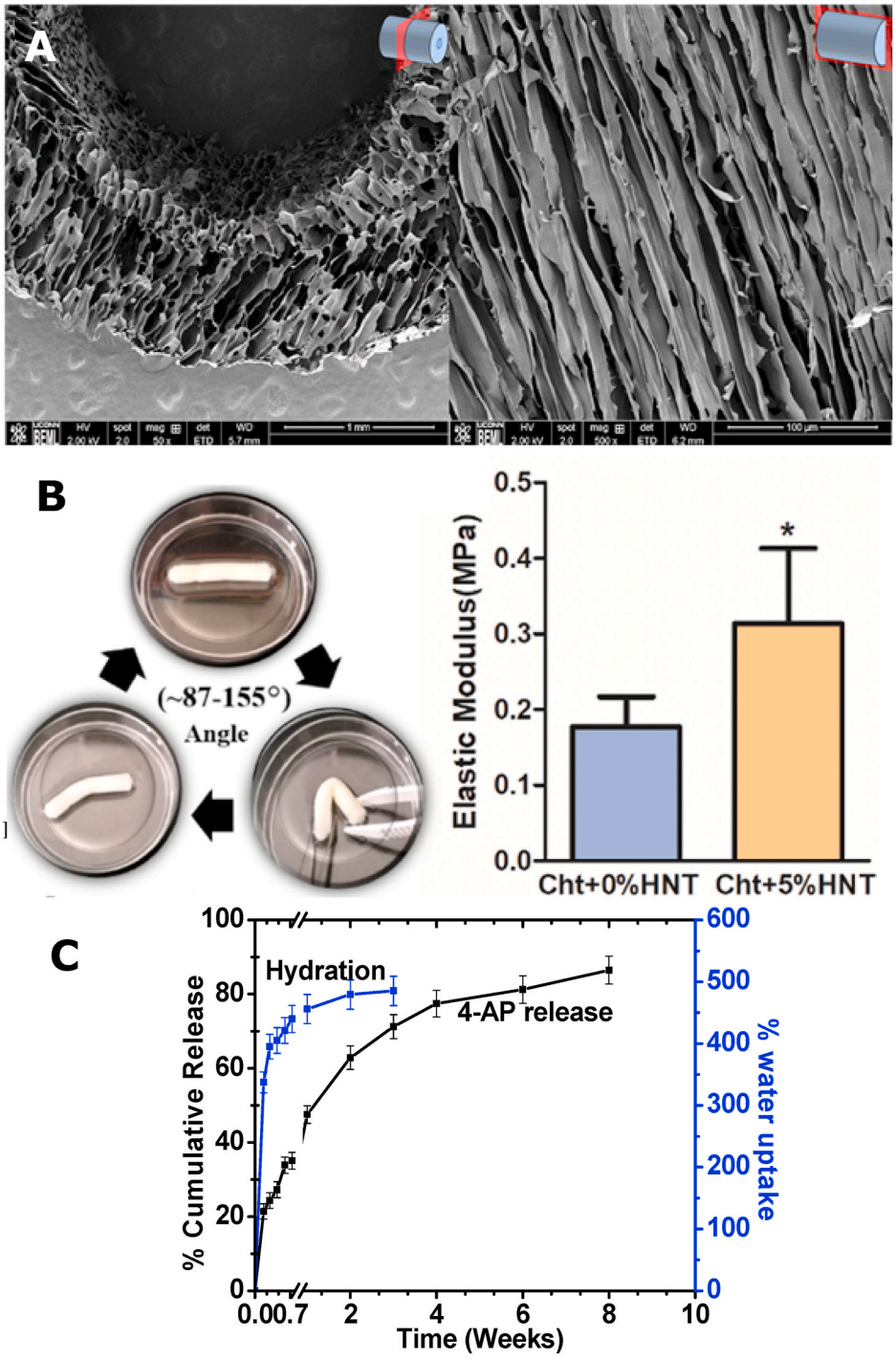

Fig. 3. Physicochemical properties of the NGCs. (*A*) SEM images of fabricated NGCs in cross section (Left; Size bar = 1 mm) and longitudinal section (Right; Size bar = 100 μm) presenting aligned microchannels. (B) These NGCs are kink-resistant (Left) and suturable, with suture retention strength ranging 18–20 N in a hydrated state. The tensile modulus (Right) of the chitosan-HNT (Cht+5% HNT) composite is higher than Cht alone (Cht+0%HNT), and both are appropriate for nerve defect repair. (C) These NGCs achieved equilibrium hydration over a week and provided a sustained release of 4-AP over a period 8 weeks. Scaffolds maintained their intact structure and strength over a period of 8 weeks in our study. All data (n = 6 per group) are shown as mean ± SEM. * = $p < 0.05$ vs control; color indicates test group comparator. (For interpretation of the references to color in this figure legend, the reader is referred to the Web version of this article.)

dysfunction, respectively. As a baseline, pre-operative SFI was measured for all rats (−10.15 ± 1.18; mean ± SEM). After surgery, there was a sharp decrease in SFI at 2 weeks post-operation for all surgical groups that was maintained through the 8-week follow-up (Fig. 4A). We did not observe any differences between the test groups (autograft, conduit, and drug-conduit); however, all test groups exhibited lower SFI than the sham surgery group at all timepoints excluding the week 0 baseline.

3.3.2. Paw area

There was a dramatic decrease in paw area 2 weeks post-operation, compared to baseline, corresponding to the limited capability of toe spread of injured rats (Fig. 4B). Given the data representation for gait testing as a percent of ipsilateral vs contralateral, a value of approximately 100% is considered normal. Paw area values may also be affected by the rat heel, which drops with nerve injury, and may form a longer footprint. Paw area did not show a marked change over the 8-week study, with no differences observed between any of the test groups (autograft, conduit, and drug conduit). However, all test groups exhibited lower paw area than sham controls at all timepoints excluding the week 0 baseline. Paw areas at 8 weeks post-operation trended slightly lower than at 2, 4, and 6 weeks, perhaps due to the relatively quicker healing of the aforementioned heel drop, which would further decrease the footprint.

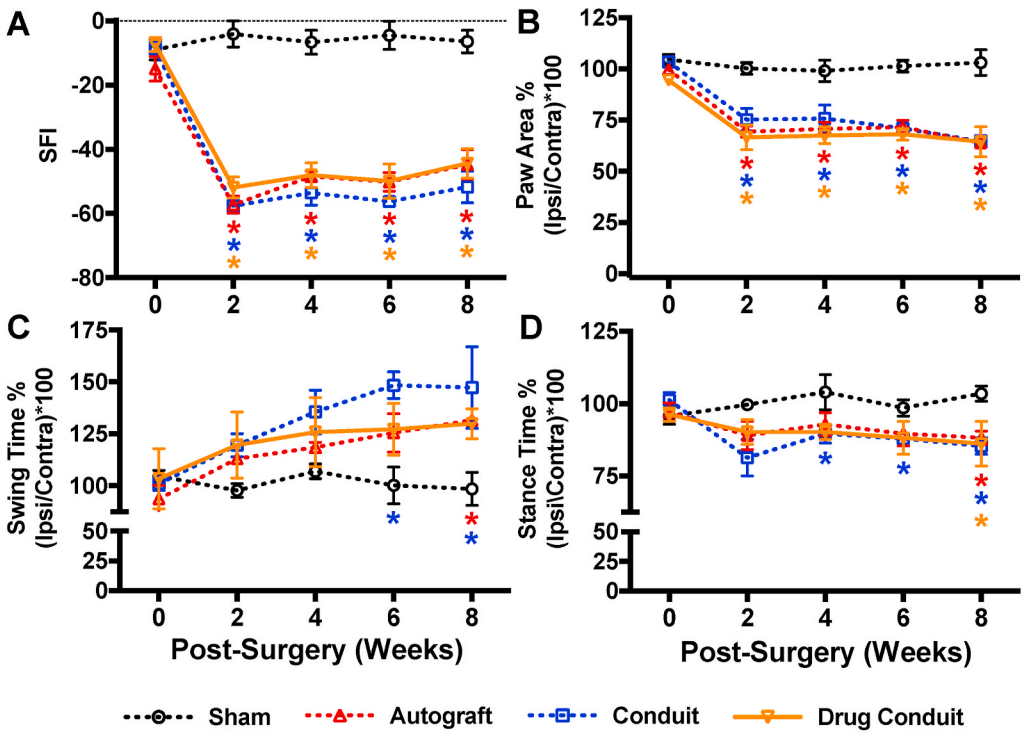

Fig. 4. Drug-conduit and autograft implants confer similar functional recovery from critical-size nerve injuries in rats. Assessment of post-operative functional recovery using walking track analysis. (*A*) Sciatic functional index (SFI) compares geometric representations of injured hind paws to contralateral uninjured paws, where values are scaled from ~-10 (representing nearly normal function) to ~ -100 (severe injury). Improvements can be seen in test groups from 2 to 8 weeks post-operation, with autograft and drug-conduit groups having nearly identical trends. (*B*) Paw area reflects the size of the paw print during the stance phase, which decreases after nerve injury. (*C*) Duration of swing phase where the paw is not in contact with the glass runway, which increases after nerve injury. (*D*) Duration of the stance phase where the paw is in contact with the glass runway, which decreases after nerve injury. Data in *B, C,* and *D* are expressed as percentages: ratios between the ipsilateral (right) hind paw and the contralateral (left) hind paw times 100. All data (n = 4–6 per group per time-point) are shown as mean ± SEM. * = p < 0.05 vs sham; color indicates test group comparator. Ipsi = ipsilateral; Contra = contralateral. (For interpretation of the references to color in this figure legend, the reader is referred to the Web version of this article.)

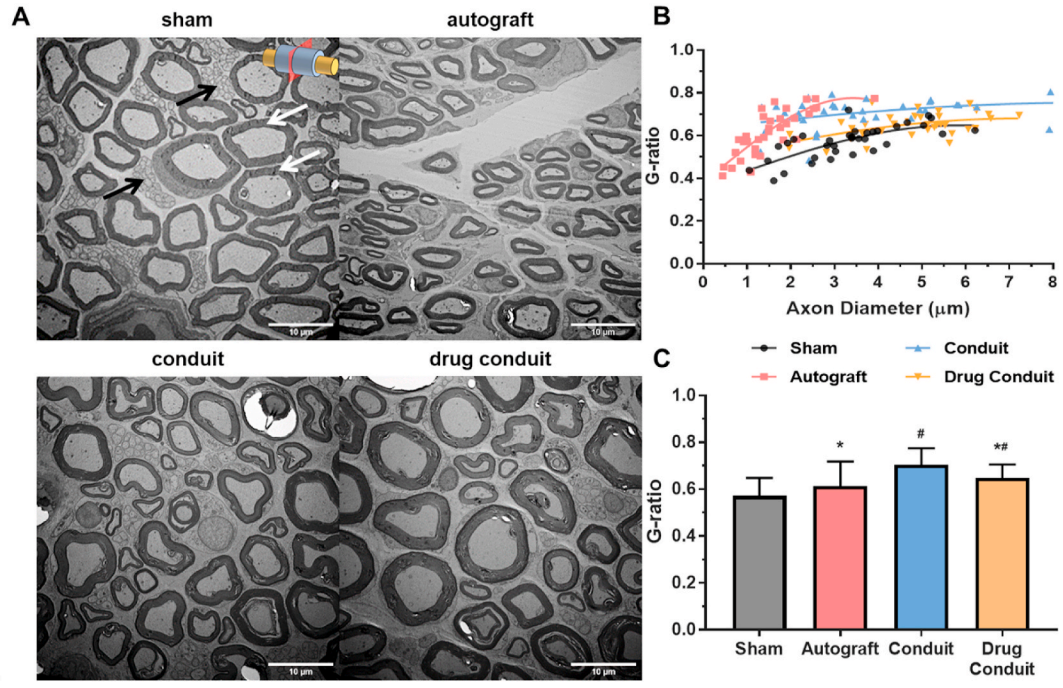

Fig. 5. Drug-conduit implants supported axon regeneration comparable with autografts at 8 weeks post-operation. (*A*) Transmission electron microscopy (TEM) of cross sections of the middle region of the regenerated sciatic nerve at 8 weeks post-operation. Black arrows indicate unmyelinated C-fiber axons and white arrows indicate myelinated A-fiber axons. Images were obtained at 1000x magnification; Size bars = 10 μm. (*B*) Scatter plot of axon diameter against G-ratio (axon diameter/fiber diameter) with logarithmic regression curves. (*C*) Test and control myelin sheath thicknesses (G-ratio). G-ratio is the ratio of inner axon diameter to outer fiber diameter where lower ratio indicates thicker myelin. Data are expressed as mean ± SD. *n* = 35 measurements per group. # = p < 0.05 vs sham, * = p < 0.05 vs conduit.

3.3.3. Swing time

Swing time refers to the period of time the foot is off of the surface, swinging forward during the gait cycle. Typically, swing time is increased as a result of injury, as animals are more reluctant to (or physically cannot) put weight on, or bear load with, the affected leg. This was quantified with the sciatic nerve transection, where at 2 weeks post-operation swing time increased for all test groups compared with sham control (Fig. 4C). Swing time usually stabilizes around 6 weeks post-operation, and at 6 weeks, we observed that conduit (only) had higher swing time than sham control, and at 8 weeks post-operation, autograft and conduit had higher swing time than sham control. Drug-conduit was no different than sham control at any time point.

3.3.4. Stance time

Stance time refers to the period of time the foot is in contact with the surface. In direct contrast with swing time, stance time is typically decreased as a result of injury. A baseline stance time was recorded for all groups (98.27 ± 0.96%; mean ± SEM) (Fig. 4D). At 4, 6, and 8 weeks post-operation, conduit exhibited the lowest stance time compared with sham controls. At 8 weeks post-operation, all test groups had lower stance time than sham controls.

3.4. Nerve morphology and myelin assessment

Nerve regeneration was observed in all test groups 8 weeks after implantation with differing degrees of myelination (Fig. 5A). A logarithmic regression between G-ratio and axon diameter detailed the relationship between the two parameters for each measured axon (Fig. 5D). Intriguingly, myelin thickness (by G-ratio) comparisons between the main treatment groups (excluding sham control) concluded that, autograft had the thickest myelin followed by drug-conduit, and conduit presented the thinnest myelin (Fig. 5C). However, only conduit and drug-conduit group myelin G-ratios were different than sham control, and autograft and drug-conduit groups were different than conduit values.

3.5. Histological evaluation

We assessed myelin presence, distribution, and amounts using Luxol fast blue, a myelin sheath stain that stains phospholipids, the main constituent of myelin. All groups showed myelin production, as seen by the characteristic light blue staining of longitudinal sections (Fig. 6A). When myelin was quantified from these images, autograft, conduit, and drug-conduit were found to be lower than sham controls; however, there were no differences between test groups (Fig. 6B). Using the same Luxol fast blue staining, we quantified the number of infiltrating cells for each group, expressed as fold change normalized to sham values (Fig. 6C), and found an increase in infiltrating immune cells for all test groups as compared with sham control, as expected. In addition, the autograft group had lower immune cell numbers than the conduit group.

In similar assessments, the presence, distribution, and amounts of neurofilament-H (NF–H) and S100 were measured using immunohistochemistry of longitudinal sections where the marker stains dark brown (Fig. 7A). NF–H staining was observed for all groups, with sham control exhibiting the highest content and the conduit group exhibiting the lowest content. These differences were confirmed by quantifying NF–H percent area, which showed that all groups had lower NF–H than sham control, and autograft and drug-conduit were similar and higher than

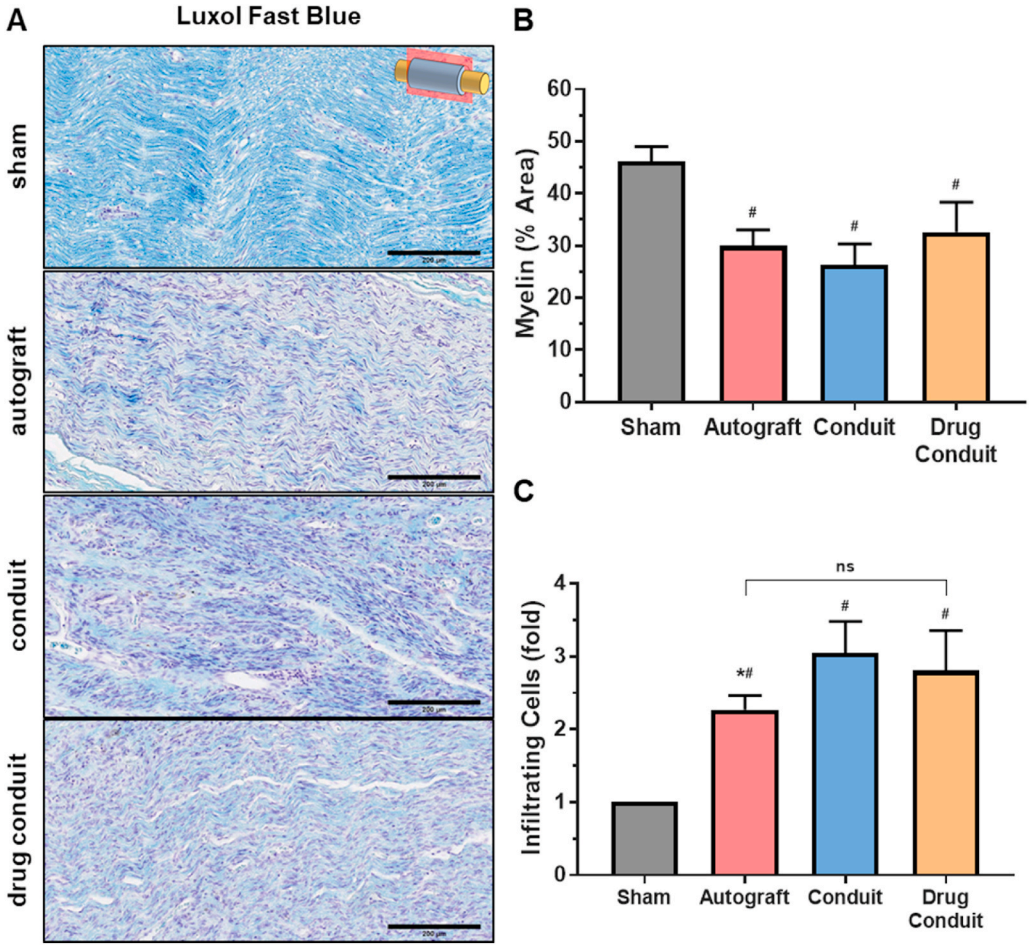

Fig. 6. Myelin production and number of infiltrating immune cells were similar between drug-conduit and autograft at 8 weeks post-operation. (*A*) Histological longitudinal sections of the middle region of the regenerated sciatic nerve stained for myelin (Luxol fast blue staining) at 8 weeks post-operation. Images were obtained at 20x magnification, where myelin is stained light blue and cell nuclei are stained violet; Size bars = 200 μm. (*B*) Quantification of average myelin area (%) from the middle region of the regenerated nerve. (*C*) Number of infiltrating immune cells normalized to the sham group and expressed as fold change. Data are expressed as mean ± SD, $n = 5$ per group. # = $p < 0.05$ vs sham, * = $p < 0.05$ vs conduit. ns = non-significant. (For interpretation of the references to color in this figure legend, the reader is referred to the Web version of this article.)

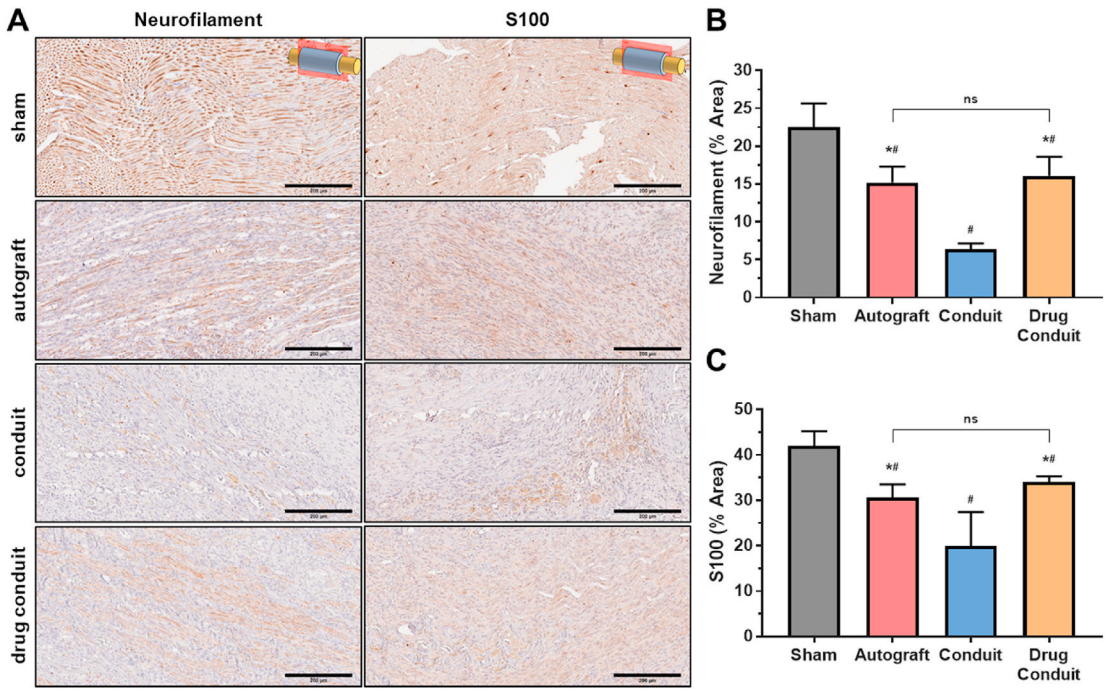

Fig. 7. Drug-conduit and autograft implants show similar neurogenic marker expression at 8 weeks post-operation. (*A*) Immunohistochemical histology assessment showing longitudinal sections of the middle region of the regenerated sciatic nerve stained for neurofilament (NF–H) and S100 at 8 weeks post-operation. Images were obtained at 20x magnification; Size bars = 200 μm. Marker proteins stain brown. (*B*) Quantification of average NF–H area (%) from the middle region of the regenerated nerve. (*C*) Quantification of average S100 area (%) from the middle region of the regenerated nerve. Data are expressed as mean ± SD, $n = 5$ per group. # = $p < 0.05$ vs sham, * = $p < 0.05$ vs conduit. ns = non-significant. (For interpretation of the references to color in this figure legend, the reader is referred to the Web version of this article.)

conduit (Fig. 7C). S100 staining showed a similar trend to that of NF–H (Fig. 7C), where all groups were lower than sham control, and autograft and drug-conduit were similar and higher than conduit.

In an effort to investigate any potential toxicity of HNTs, cross-sections of rat liver tissue were stained with H&E. Fig. 8 shows the histological assessment of hepatic tissues harvested from sham, autograft, conduit, and drug-conduit groups. The hepatic tissues in the control animals (sham and autograft) and the conduit and drug-conduit test groups showed normal hepatic architecture [53], revealing that HNTs at the given dose had no remarkable adverse effects on the liver. No fatty degeneration, local hydropic degeneration, or spotted necrosis was observed in the hepatic tissue of conduit or drug-conduit groups, which may occur with HNT administration at particularly high doses, where systemic clearance and excretion is not sufficient [53–55]. A

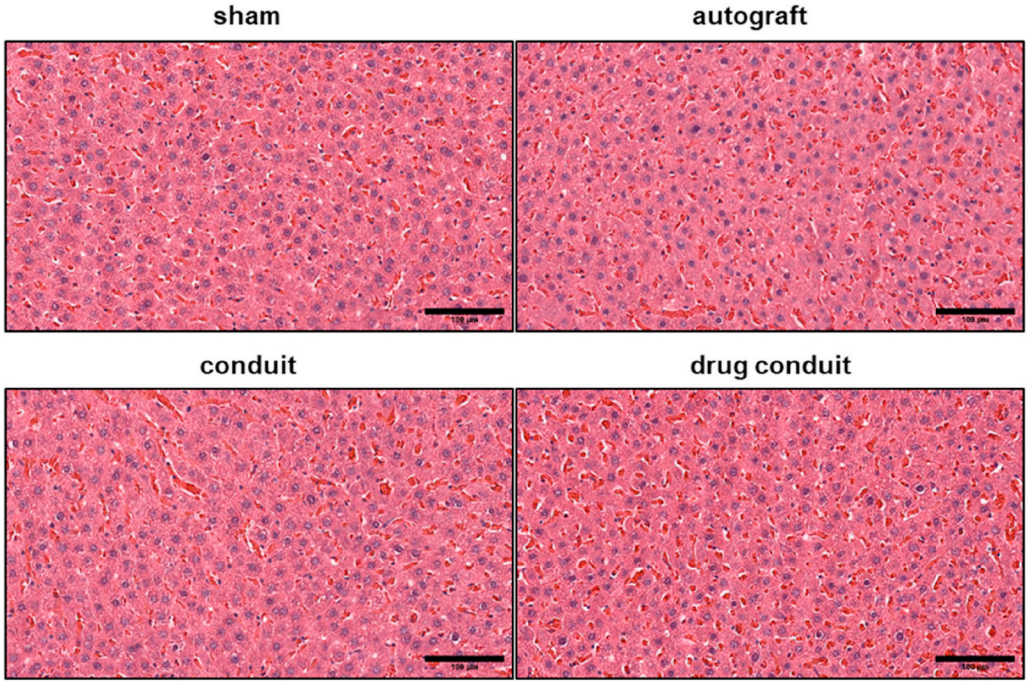

Fig. 8. No apparent hepatotoxicity was observed in HNT-containing conduits or any test group. Histological cross sections (H&E stain) of liver tissue in rats 8 weeks post-operation were used to assess potential toxicity of HNT conduits. Sham and autograft groups do not contain chitosan or HNTs. No fatty degeneration, local hydropic degeneration, or spotted necrosis was observed in the hepatic tissue of conduit or drug-conduit groups, which may occur with higher doses of any excess material or bioactive factor administration, where systemic clearance and excretion is not sufficient. Size bar = 100 μm.

representative photograph of the regenerated sciatic nerve from a rat at 8 weeks post-operation within the center of the scaffold (cut in cross-section) further confirms the axon bridging (Fig. 9). The NGC can be seen in the darker yellow/amber color, where the native proximal nerve is shown at the top in white. Regenerated nerve can be seen growing from the center of the tubular conduit.

4. Discussion

The ultimate goal of all nerve repair and regeneration strategies is reestablishing continuation of the nerve channel to reinnervate the target tissue and conduct electrical impulses. Our aligned conduit construct, delivering a sustained release of 4-AP, showed successful nerve repair and regeneration, both histologically and functionally, showing regenerative efficacy equal to that of the gold-standard autograft. The critical-size sciatic nerve transection is a severe PNI model that results in significant sensory and motor loss of the hindlimb. Autologous nerve grafting (autograft) is considered to be the gold-standard treatment for PNI with a large segmented gap [56]. Due to several disadvantages of autografts, engineered nerve conduits have been developed as alternatives for segmental PNI treatment. Recent studies have shown the ability of NGCs to improve the repair and regeneration across a nerve gap, with marked increases in functional recovery, which was also shown in our study [57–59].

Chitosan is a natural, biodegradable, and versatile biopolymer that is highly biocompatible and effectively used in antibacterial, antifungal, and regenerative medicine applications [60–62]. The development of chitosan scaffolds for tissue engineering and regenerative medicine applications has been extensively studied with great successes, despite poor mechanical integrity [60–62]. To combat such disadvantages, chitosan scaffolds can be doped with supporting compounds to create mechanically competent composites. Biopolymers are often doped with nanofillers that increase scaffold mechanical strength, but can also enhance biological compatibility by promoting cell adhesion due to the surface irregularities of the scaffold pores; these arise due to the insoluble nanofillers [63]. Our previous work details the doping of conduits with HNTs. HNTs can have lengths ranging from 0.3 to 1.5 μm, with an inner lumen diameter of ~40–70 nm [19]. The neighboring alumina and silica layers, with differing waters of hydration, curve and form multilayer tubes due to a packing disorder. The innermost alumina surface is positively charged, while the outermost silicate surface is negatively charged [64]. The hollow lumen of HNTs provides excellent ability to carry, encapsulate, and transport drugs and biomacromolecules, so they can effectively sustain drug release while also controlling burst release characteristics of smaller hydrophilic molecules. When mixed with cationic chitosan in a dilute acidic solution, the negatively-charged HNTs form a chitosan-HNT complex via electrostatic interactions. Furthermore, halloysite can form hydrogen bonds with the amino- and hydroxyl-groups of chitosan, further increasing the interfacial compatibility and dispersion of HNTs in chitosan [64].

Typically, after severing the sciatic nerve, a rat is unable to walk normally on its toes. As a result, the heel drops and forms a long footprint, until reinnervation of the nerve is established and muscle function is returned [49]. Post-injury, there is also a noticeable collapse of the

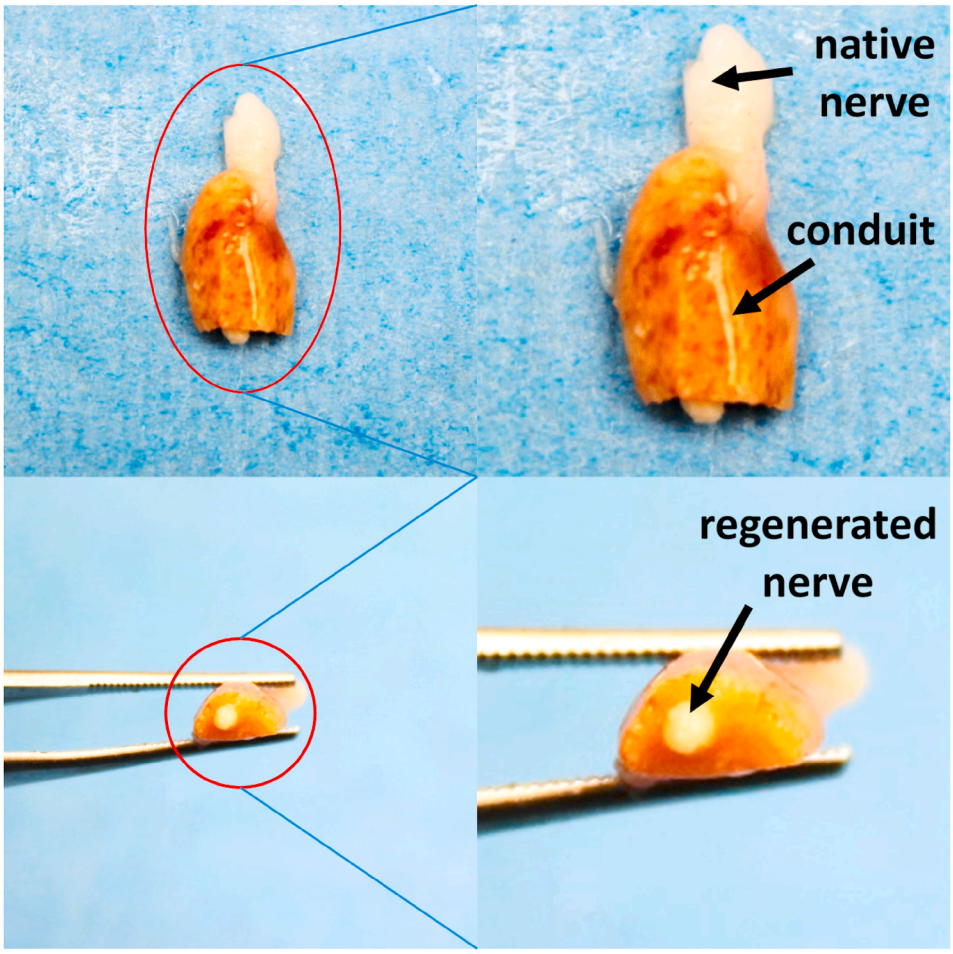

Fig. 9. A representative photograph shows the center, regenerated region of the sciatic nerve from a rat at 8 weeks post-operation cut in cross-section. The NGC can be seen in the darker yellow/amber color, where the native proximal nerve is shown at the top in white. Regenerated nerve can be seen growing from the center of the tubular conduit. (For interpretation of the references to color in this figure legend, the reader is referred to the Web version of this article.)

affected limb toe spread that is slowly restored with regeneration of the sciatic nerve. Taking advantage of such post-injury changes, the calculation of SFI serves as a strong indicator for functional recovery of the sciatic nerve. We observed a sharp reduction in SFI post-surgery, and SFI noticeably increased over the 8-week test period. The equivalency of autograft and drug-conduit groups at 8 weeks post-operation is a strong positive indicator of the efficacy of the drug-conduit. Neat (no-drug) conduit groups did not show any statistical differences from autograft or drug-conduit groups in functional assessments, which may reflect the functional capabilities of the aligned microchannel pores to physically guide regenerating axons and improve target reinnervation. Autograft and drug-conduit groups performed virtually identically for paw area, swing time, and stance time, further confirming the drug-conduit's ability to improve functional recovery post-nerve transection.

The endogenous repair of transected PNI is marked by three broad phases: Wallerian degeneration, axonal regeneration, and target-organ reinnervation. Schwann cells are vital primary mediators of the cascading events of Wallerian degeneration, including the recruitment of macrophages, along with increases in critical factors such as BDNF and NGF [65–67]. The ability of the small-molecule drug 4-AP to increase BDNF and NGF release in Schwann cells *in vitro* was shown in a previous publication [19]. The protein marker S100 exists only in glial cells of the central nervous system and Schwann cells of the peripheral nervous system. Many S100-positive Schwann cells were observed via immunohistochemical staining in all groups, with autograft and drug-conduit groups showing relatively equal levels of S100, significantly greater than neat (no-drug) conduit groups. The increased expression of S100 may be a result of increased Schwann cell recruitment to the injury site due to chemotactic effects of amplified neurotransmitter release as a direct result of 4-AP administration. This trend was also seen with the detection of NF–H, a neurofilament protein that is a primary component of the mature neuronal cytoskeleton, and significantly downregulated at the early period following axonal transection [68]. When NF–H-positive axons were quantified, levels were not significantly different between autograft and drug-conduit groups, which both showed higher levels than neat (no-drug) conduit groups.

The degree of repair and regeneration achieved by the nerve conduit was further confirmed by the investigation of myelin production and thickness, both histologically and using TEM. Using a Luxol fast blue stain for myelin, histological studies revealed abundant, well-myelinated axons in the mid-portion of the regenerated nerve. Autograft groups showed no statistical differences compared to both neat (no-drug) conduit and drug-conduit groups. Similarly, in TEM morphometric studies, myelin thickness was equivalent between autograft and drug-conduit groups, which were significantly greater than neat (no-drug) conduit groups (smaller G-ratio). This is perhaps attributed to the ability of 4-AP to upregulate the release of myelin proteins in Schwann cells, including P0, which was shown in our previous publication [19].

Despite the successes of the current study, there are several limitations. Firstly, due to greater variability in functional assessments, the number of animals in each group may need to be increased to obtain more walking track data points, which may help in the identification of statistically significant improvements between groups. Second, it is possible that functional differences between groups, specifically the neat (no-drug) conduit and drug-conduit, may be evident at later time points given the differences observed in TEM and histology between these groups at the 8-week post-operative time point. Thus, extending the study to include later timepoints may yield more evident changes and improvements in functional recovery. Nevertheless, the functional assessments provided key insights into differences between the groups, and highlighted the performance equivalence between the control autograft and test drug-conduit. Third, the release of 4-AP was not quantified and characterized *in vivo*. The quantification and optimization of 4-AP released *in vivo* will be critical to harness the full capabilities of this drug for optimized nerve regeneration. According to the pathophysiology of peripheral nerve injury and repair, the first 7–21 days offer the greatest potential for facilitated regeneration as this is the period of Wallerian degeneration, cell recruitment, and the beginning of axonal regeneration. As such, this will be the period where 4-AP will have the greatest functional impacts. Previous *in vitro* studies we show feasibility of sustained release well over 14 days [19], however the dosing of drug in the implanted conduits should be evaluated, modified, and optimized in future studies.

We conducted several extensive studies and assessments to evaluate peripheral nerve regeneration using our previously developed and characterized NGC. The advantages of our NGC are [1] the aligned microchannel porosity, which can physically guide the regenerating axons across the injury gap for better distal target reinnervation; and [2] the sustained release of the small-molecule drug 4-AP, which can increase nerve conduction, increasing the release of synaptic neurotransmitters and critical Schwann cell neurotrophic factors including BDNF, NGF, and P0. We observed varying levels of nerve regeneration across the autograft, conduit, and drug-conduit groups. All three groups showed successful increases in functional recovery without significant differences; however, the drug-conduit outperformed the neat (no drug) conduit in terms of histological and morphometric evaluations of myelin, S100, and NF–H. Overall, the drug-conduit showed equivalency to autograft repair in a majority of the functional, morphological, and histological assessments. These results indicate the success of the conduit's aligned microchannel architecture to facilitate physical guidance and reinnervation, but also highlight the enhanced efficacy of regeneration achieved by the drug-conduit, a testament to the contributions of 4-AP to the repair and regeneration process. This represents a significant advance in the fields of peripheral nerve repair, regeneration, and engineering, where an aligned NGC was shown to be a clinically feasible drug delivery vehicle for small molecule drug 4-AP *in vivo*, with a strong ability to treat PNI.

5. Conclusion

The present study looked at novel NGCs with aligned microchannel pores delivering a sustained release of 4-AP for peripheral nerve regeneration in a critical-size rat sciatic nerve transection model. The results of functional walking track analysis, morphometric evaluations of myelin development, and histological assessments of various markers confirmed the equivalency of drug-conduit repair to autograft control treatment. The conduit's aligned microchannel architecture may play a vital role in facilitating physical guidance and distal target reinnervation, while the sustained release of 4-AP may increase nerve conduction, and in turn synaptic neurotransmitter release and upregulation of critical Schwann cell neurotrophic factors. This facilitates more efficient and efficacious peripheral nerve regeneration via a drug delivery system that is feasible for clinical application.

CRediT authorship contribution statement

Ohan S. Manoukian: Conceptualization, Data curation, Formal analysis, Methodology, Writing - review & editing. **Swetha Rudraiah:** Formal analysis, Methodology. **Michael R. Arul:** Methodology. **Jenna M. Bartley:** Methodology. **Jiana T. Baker:** Methodology. **Xiaojun Yu:** Formal analysis. **Sangamesh G. Kumbar:** Conceptualization, Data curation, Formal analysis, Methodology, Project administration, Supervision, Funding acquisition, Writing - review & editing.

Declaration of competing interest

There is No conflict of interest to publish this research article.

Acknowledgements

The authors acknowledge funding support from the National

Institute of Biomedical Imaging and Bioengineering of the National Institutes of Health (R01EB020640) and Department of Defense through the Peer Reviewed Orthopaedic Research Program under Award No. [W81XWH-13-1-0320]. Ohan S. Manoukian is the recipient of the National Science Foundation (NSF) Graduate Research Fellowship (Grant No. DGE-1747453). The authors would like to thank Kit Bonin and Geneva Hargis for help editing our manuscript.

References

[1] K. Brattain, ANALYSIS OF THE PERIPHERAL NERVE REPAIR MARKET IN THE UNITED STATES, 2013.
[2] R.M. Menorca, T.S. Fussell, J.C. Elfar, Peripheral nerve trauma: mechanisms of injury and recovery, Hand Clin. 29 (3) (2013) 317.
[3] X. Jiang, S.H. Lim, H.-Q. Mao, S.Y. Chew, Current applications and future perspectives of artificial nerve conduits, Exp. Neurol. 223 (1) (2010) 86–101.
[4] A.M. Moore, M. MacEwan, K.B. Santosa, K.E. Chenard, W.Z. Ray, D.A. Hunter, S. E. Mackinnon, P.J. Johnson, Acellular nerve allografts in peripheral nerve regeneration: a comparative study, Muscle Nerve 44 (2) (2011) 221–234.
[5] M. Anderson, N.B. Shelke, O.S. Manoukian, X. Yu, L.D. McCullough, S.G. Kumbar, Peripheral nerve regeneration strategies: electrically stimulating polymer based nerve growth conduits, Crit. Rev. Biomed. Eng. 43 (2–3) (2015) 131–159, https://doi.org/10.1615/CritRevBiomedEng.2015014015. Epub 2015/01/01, PubMed PMID: 27278739; PMCID: PMC5266796.
[6] J. Moskow, B. Ferrigno, N. Mistry, D. Jaiswal, K. Bulsara, S. Rudraiah, S. G. Kumbar, Bioengineering approach for the repair and regeneration of peripheral nerve, Bioact. Mater. 4 (2019) 107–113.
[7] P. Chrząszcz, K. Derbisz, K. Suszyński, J. Miodoński, R. Trybulski, J. Lewin-Kowalik, W. Marcol, Application of peripheral nerve conduits in clinical practice: a literature review, Neurol. Neurochir. Pol. 52 (4) (2018) 427–435.
[8] P.A. Wieringa, A.R. Gonçalves de Pinho, S. Micera, R.J. van Wezel, L. Moroni, Biomimetic architectures for peripheral nerve repair: a review of biofabrication strategies, Adv. Healthc. Mater. 7 (8) (2018) 1701164.
[9] B. Guo, P.X. Ma, Conducting polymers for tissue engineering, Biomacromolecules 19 (6) (2018) 1764–1782.
[10] E.O. Johnson, P.N. Soucacos, Nerve repair: experimental and clinical evaluation of biodegradable artificial nerve guides, Injury 39 (3) (2008) 30–36.
[11] O.S. Manoukian, J.T. Baker, S. Rudraiah, M.R. Arul, A.T. Vella, A.J. Domb, S. G. Kumbar, Functional polymeric nerve guidance conduits and drug delivery strategies for peripheral nerve repair and regeneration, J. Contr. Release 317 (2020) 78–95.
[12] B. Ferrigno, R. Bordett, N. Duraisamy, J. Moskow, M.R. Arul, S. Rudraiah, S. P. Nukavarapu, A.T. Vella, S.G. Kumbar, Bioactive polymeric materials and electrical stimulation strategies for musculoskeletal tissue repair and regeneration, Bioact. Mater. 5 (3) (2020) 468–485, https://doi.org/10.1016/j.bioactmat.2020.03.010. Epub 2020/04/14, PubMed PMID: 32280836; PMCID: PMC7139146.
[13] M. Zheng, J. Guo, Q. Li, J. Yang, Y. Han, H. Yang, M. Yu, L. Zhong, D. Lu, L. Li, Syntheses and characterization of anti-thrombotic and anti-oxidative Gastrodin-modified polyurethane for vascular tissue engineering, Bioact. Mater. 6 (2) (2021) 404–419.
[14] P. Chen, X. Piao, P. Bonaldo, Role of macrophages in Wallerian degeneration and axonal regeneration after peripheral nerve injury, Acta Neuropathol. 130 (5) (2015) 605–618.
[15] O.A. Sulaiman, T. Gordon, Effects of short-and long-term Schwann cell denervation on peripheral nerve regeneration, myelination, and size, Glia 32 (3) (2000) 234–246.
[16] B.J. Pfister, T. Gordon, J.R. Loverde, A.S. Kochar, S.E. Mackinnon, D.K. Cullen, Biomedical engineering strategies for peripheral nerve repair: surgical applications, state of the art, and future challenges, Crit. Rev. Biomed. Eng. 39 (2) (2011).
[17] A. Bozkurt, R. Deumens, C. Beckmann, L.O. Damink, F. Schügner, I. Heschel, B. Sellhaus, J. Weis, W. Jahnen-Dechent, G.A. Brook, In vitro cell alignment obtained with a Schwann cell enriched microstructured nerve guide with longitudinal guidance channels, Biomaterials 30 (2) (2009) 169–179.
[18] W. Chang, M.B. Shah, G. Zhou, K. Walsh, S. Rudraiah, S.G. Kumbar, X. Yu, Polymeric nanofibrous nerve conduits coupled with laminin for peripheral nerve regeneration, Biomed. Mater. 15 (3) (2020), 035003, https://doi.org/10.1088/1748-605X/ab6994. Epub 2020/01/10, PubMed PMID: 31918424; PMCID: PMC7199806.
[19] O.S. Manoukian, M.R. Arul, S. Rudraiah, I. Kalajzic, S.G. Kumbar, Aligned microchannel polymer-nanotube composites for peripheral nerve regeneration: small molecule drug delivery, J. Contr. Release : Off. J. Contr. Release Soc. 296 (2019) 54–67, https://doi.org/10.1016/j.jconrel.2019.01.013. Epub 2019/01/19, PubMed PMID: 30658124; PMCID: PMC6379151.
[20] S.W. Kemp, A.A. Webb, S. Dhaliwal, S. Syed, S.K. Walsh, R. Midha, Dose and duration of nerve growth factor (NGF) administration determine the extent of behavioral recovery following peripheral nerve injury in the rat, Exp. Neurol. 229 (2) (2011) 460–470, https://doi.org/10.1016/j.expneurol.2011.03.017. Epub 2011/04/05, PubMed PMID: 21458449.
[21] A.C. Lee, V.M. Yu, J.B. Lowe 3rd, M.J. Brenner, D.A. Hunter, S.E. Mackinnon, S. E. Sakiyama-Elbert, Controlled release of nerve growth factor enhances sciatic nerve regeneration, Exp. Neurol. 184 (1) (2003) 295–303.
[22] E. Vogelin, J.M. Baker, J. Gates, V. Dixit, M.A. Constantinescu, N.F. Jones, Effects of local continuous release of brain derived neurotrophic factor (BDNF) on peripheral nerve regeneration in a rat model, Exp. Neurol. 199 (2) (2006) 348–353.
[23] C. Zhan, C.B. Ma, H.M. Yuan, B.Y. Cao, J.J. Zhu, Macrophage-derived microvesicles promote proliferation and migration of Schwann cell on peripheral nerve repair, Biochem. Biophys. Res. Commun. 468 (1–2) (2015) 343–348.
[24] J. McBride, D. Smith, S. Byrn, R. Borgens, R. Shi, 4-Aminopyridine derivatives enhance impulse conduction in Guinea-pig spinal cord following traumatic injury, Neuroscience 148 (1) (2007) 44–52.
[25] K. Moriguchi, K. Miyamoto, S. Kusunoki, 4-Aminopyridine ameliorates experimental autoimmune neuritis in Lewis rats, J. Neuroimmunol. 305 (2017) 72–74.
[26] K.C. Tseng, H. Li, A. Clark, L. Sundem, M. Zuscik, M. Noble, J. Elfar, 4-Aminopyridine promotes functional recovery and remyelination in acute peripheral nerve injury, EMBO Mol. Med. 8 (12) (2016) 1409–1420.
[27] M. Noble, K.-C. Tseng, H. Li, J.C. Elfar, 4-Aminopyridine as a single agent diagnostic and treatment for severe nerve crush injury, Mil. Med. 184 (Supplement_1) (2019) 379–385.
[28] M.E. Shy, Peripheral neuropathies caused by mutations in the myelin protein zero, J. Neurol. Sci. 242 (1–2) (2006) 55–66.
[29] H.B. Jensen, M. Ravnborg, U. Dalgas, E. Stenager, 4-Aminopyridine for symptomatic treatment of multiple sclerosis: a systematic review, Therapeut. Adv. Neurol. Disord. 7 (2) (2014) 97–113.
[30] S.I. Judge, C.T. Bever, Potassium channel blockers in multiple sclerosis: neuronal K v channels and effects of symptomatic treatment, Pharmacol. Ther. 111 (1) (2006) 224–259.
[31] R. Sherratt, H. Bostock, T. Sears, Effects of 4-aminopyridine on normal and demyelinated mammalian nerve fibres, Nature 283 (5747) (1980) 570–572.
[32] E.S. Anton, G. Weskamp, L.F. Reichardt, W.D. Matthew, Nerve growth factor and its low-affinity receptor promote Schwann cell migration, Proc. Natl. Acad. Sci. Unit. States Am. 91 (7) (1994) 2795–2799.
[33] R.M. Lindsay, Nerve growth factors (NGF, BDNF) enhance axonal regeneration but are not required for survival of adult sensory neurons, J. Neurosci. 8 (7) (1988) 2394–2405.
[34] J.M. Cosgaya, J.R. Chan, E.M. Shooter, The neurotrophin receptor p75NTR as a positive modulator of myelination, Science 298 (5596) (2002) 1245–1248.
[35] J.Y. Zhang, X.G. Luo, C.J. Xian, Z.H. Liu, X.F. Zhou, Endogenous BDNF is required for myelination and regeneration of injured sciatic nerve in rodents, Eur. J. Neurosci. 12 (12) (2000) 4171–4180.
[36] S-i Yamaguchi, M.A. Rogawski, Effects of anticonvulsant drugs on 4-aminopyridine-induced seizures in mice, Epilepsy Res. 11 (1) (1992) 9–16.
[37] R. Yendluri, D.P. Otto, M.M. De Villiers, V. Vinokurov, Y.M. Lvov, Application of halloysite clay nanotubes as a pharmaceutical excipient, Int. J. Pharm. 521 (1–2) (2017) 267–273.
[38] Q. Quan, H. Meng, B. Chang, L. Hong, R. Li, G. Liu, X. Cheng, H. Tang, P. Liu, Y. Sun, Novel 3-D helix-flexible nerve guide conduits repair nerve defects, Biomaterials 207 (2019) 49–60.
[39] M.S. Firouzi, M. Firouzi, M.H. Nabian, L.O. Zanjani, S.A. Zadegan, R.S. Kamrani, V. Rahimi-Movaghar, The effects of picric acid (2, 4, 6-trinitrophenol) and a bite-deterrent chemical (denatonium benzoate) on autotomy in rats after peripheral nerve lesion, Lab. Anim. 44 (4) (2015) 141.
[40] R.A. Weber, W.H. Proctor, M.R. Warner, C.N. Verheyden, Autotomy and the sciatic functional index, Microsurgery 14 (5) (1993) 323–327.
[41] F.M. Pestana, R.C. Domingues, J.T. Oliveira, D.F. Durço, C.O. Goulart, H. R. Mendonça, A.C.R. dos Santos, N.T. de Campos, B.T. da Silva, C.C. Pereira, Comparison of morphological and functional outcomes of mouse sciatic nerve repair with three biodegradable polymer conduits containing poly (lactic acid), Neural Regen. Res. 13 (10) (2018) 1811.
[42] C.O. Goulart, F.R.P. Lopes, Z.O. Monte, S.V. Dantas Jr., A. Souto, J.T. Oliveira, F. M. Almeida, C. Tonda-Turo, C.C. Pereira, C.P. Borges, Evaluation of biodegradable polymer conduits–poly (L-lactic acid)–for guiding sciatic nerve regeneration in mice, Methods 99 (2016) 28–36.
[43] R. Bamba, D.C. Riley, J.S. Kim, N.L. Cardwell, A.C. Pollins, R.B. Shack, W. P. Thayer, Evaluation of a nerve fusion technique with polyethylene glycol in a delayed setting after nerve injury, J. Hand Surg. 43 (1) (2018) 82, e1-. e7.
[44] M.-H. Hong, H.J. Hong, H. Pang, H.-J. Lee, S. Yi, W.-G. Koh, Controlled release of growth factors from multilayered fibrous scaffold for functional recoveries in crushed sciatic nerve, ACS Biomater. Sci. Eng. 4 (2) (2018) 576–586.
[45] J.R. Bain, S.E. Mackinnon, D.A. Hunter, Functional evaluation of complete sciatic, peroneal, and posterior tibial nerve lesions in the rat, Plast. Reconstr. Surg. 83 (1) (1989) 129–138. Epub 1989/01/01. PubMed PMID: 2909054.
[46] R. Sridharan, R.B. Reilly, C.T. Buckley, Decellularized grafts with axially aligned channels for peripheral nerve regeneration, J. Mech. Behav. Biomed. Mater. 41 (2015) 124–135.
[47] C. Brandt-Wunderlich, C. Schwerdt, P. Behrens, N. Grabow, K.-P. Schmitz, W. Schmidt, A method to determine the kink resistance of stents and stent delivery systems according to international standards, Curr. Dir. Biomed. Eng. 2 (1) (2016) 289–292.
[48] Y. Lvov, W. Wang, L. Zhang, R. Fakhrullin, Halloysite clay nanotubes for loading and sustained release of functional compounds, Adv. Mater. 28 (6) (2016) 1227–1250.
[49] J. Chang, G. Gupta, Tissue Engineering for the Hand: Research Advances and Clinical Applications, World Scientific, 2010.
[50] C. Murray, Amputation, Prosthesis Use, and Phantom Limb Pain: an Interdisciplinary Perspective, Springer, 2009.

[51] X. Navarro, M. Butí, E. Verdú, Autotomy prevention by amitriptyline after peripheral nerve section in different strains of mice, Restor. Neurol. Neurosci. 6 (2) (1994) 151–157.
[52] M. Carr, T. Best, S. Mackinnon, P. Evans, Strain differences in autotomy in rats undergoing sciatic nerve transection or repair, Ann. Plast. Surg. 28 (6) (1992) 538–544.
[53] X. Wang, J. Gong, Z. Gui, T. Hu, X. Xu, Halloysite nanotubes-induced Al accumulation and oxidative damage in liver of mice after 30-day repeated oral administration, Environ. Toxicol. 33 (6) (2018) 623–630.
[54] G.I. Fakhrullina, F.S. Akhatova, Y.M. Lvov, R.F. Fakhrullin, Toxicity of halloysite clay nanotubes in vivo: a Caenorhabditis elegans study, Environ. Sci.: Nano 2 (1) (2015) 54–59.
[55] M. Kryuchkova, A. Danilushkina, Y. Lvov, R. Fakhrullin, Evaluation of toxicity of nanoclays and graphene oxide in vivo: a Paramecium caudatum study, Environ. Sci.: Nano 3 (2) (2016) 442–452.
[56] G. Lundborg, A 25-year perspective of peripheral nerve surgery: evolving neuroscientific concepts and clinical significance, J. Hand Surg. 25 (3) (2000) 391–414.
[57] V. Chiono, C. Tonda-Turo, Trends in the design of nerve guidance channels in peripheral nerve tissue engineering, Prog. Neurobiol. 131 (2015) 87–104.
[58] W.A. Lackington, A.J. Ryan, F.J. O'Brien, Advances in nerve guidance conduit-based therapeutics for peripheral nerve repair, ACS Biomater. Sci. Eng. 3 (7) (2017) 1221–1235.
[59] C. Huang, Y. Ouyang, H. Niu, N. He, Q. Ke, X. Jin, D. Li, J. Fang, W. Liu, C. Fan, Nerve guidance conduits from aligned nanofibers: improvement of nerve regeneration through longitudinal nanogrooves on a fiber surface, ACS Appl. Mater. Interfaces 7 (13) (2015) 7189–7196.
[60] S. Kumbar, A. Kulkarni, T. Aminabhavi, Crosslinked chitosan microspheres for encapsulation of diclofenac sodium: effect of crosslinking agent, J. Microencapsul. 19 (2) (2002) 173–180.
[61] A.A. Nada, R. James, N.B. Shelke, M.D. Harmon, H.M. Awad, R.K. Nagarale, S. G. Kumbar, A smart methodology to fabricate electrospun chitosan nanofiber matrices for regenerative engineering applications, Polym. Adv. Technol. 25 (5) (2014) 507–515.
[62] F. Croisier, C. Jérôme, Chitosan-based biomaterials for tissue engineering, Eur. Polym. J. 49 (4) (2013) 780–792.
[63] D. Kai, M.P. Prabhakaran, B. Stahl, M. Eblenkamp, E. Wintermantel, S. Ramakrishna, Mechanical properties and in vitro behavior of nanofiber–hydrogel composites for tissue engineering applications, Nanotechnology 23 (9) (2012), 095705.
[64] E.A. Naumenko, I.D. Guryanov, R. Yendluri, Y.M. Lvov, R.F. Fakhrullin, Clay nanotube–biopolymer composite scaffolds for tissue engineering, Nanoscale 8 (13) (2016) 7257–7271.
[65] B.D. Trapp, P. Hauer, G. Lemke, Axonal regulation of myelin protein mRNA levels in actively myelinating Schwann cells, J. Neurosci. 8 (9) (1988) 3515–3521.
[66] F.V. White, A.D. Toews, J.F. Goodrum, D.L. Novicki, T.W. Bouldin, P. Morell, Lipid metabolism during early stages of Wallerian degeneration in the rat sciatic nerve, J. Neurochem. 52 (4) (1989) 1085–1092.
[67] R. Pellegrino, M. Politis, J. Ritchie, P. Spencer, Events in degenerating cat peripheral nerve: induction of Schwann cell S phase and its relation to nerve fibre degeneration, J. Neurocytol. 15 (1) (1986) 17–28.
[68] P.N. Hoffman, S.C. Pollock, G.G. Striph, Altered gene expression after optic nerve transection: reduced neurofilament expression as a general response to axonal injury, Exp. Neurol. 119 (1) (1993) 32–36.